

Comparing hysteretic behavior of light-gauge steel plate shear walls and braced frames

Jeffrey W. Berman^a, Oguz C. Celik^{a,b,*}, Michel Bruneau^c

^aDepartment of Civil, Structural, and Environmental Engineering, University at Buffalo, Amherst, NY 14260, United States

^bDivision of Theory of Structures, Faculty of Architecture, Istanbul Technical University, Taskisla, Taksim, Istanbul 34437, Turkey

^cMultidisciplinary Center for Earthquake Engineering Research, Department of Civil, Structural, and Environmental Engineering, University at Buffalo, Amherst, NY 14260, United States

Received 12 July 2004; received in revised form 26 October 2004; accepted 15 November 2004

Available online 8 January 2005

Abstract

Braced frames and steel plate shear walls (SPSWs) have both been shown to be useful in the seismic retrofit of buildings. While both these systems have merit, no guidance exists to help the engineer determine which of the two approaches is preferable in terms of providing stiffness, maximum displacement ductility, cumulative hysteretic energy dissipation, and energy dissipation per cycle for a given strength. In an attempt to provide some quantitative data and insight for this purpose, this paper describes and compares the results from cyclic testing of six frames: four concentrically braced frames (two with cold-formed steel studs for in-plane and out-of-plane restraint of the braces and two without), and two light-gauge steel plate shear walls (one with a flat infill plate and one with a corrugated infill). The largest initial stiffness was provided by a braced frame specimen with cold formed steel studs and the largest ductility was achieved with a steel plate shear wall with flat infill. After scaling the hysteretic results to the same design base shear, it was found that both the energy dissipated per cycle and the cumulative energy dissipation were similar for flat plate SPSW and braced frames with two tubular braces, up to a ductility of four. After that the tubular braces fractured while the SPSW with a flat infill reached a ductility of nine before the energy dissipation per cycle decreased.

© 2004 Elsevier Ltd. All rights reserved.

Keywords: Steel plate shear walls; Steel braces; Cyclic testing; Hysteretic energy dissipation; Ductile retrofit

1. Introduction

The seismic retrofit of existing buildings is a difficult task due to many factors, such as architectural constraints, the cost of possibly closing the building (or part of it) for the duration of the retrofit work, or having to heavily reinforce existing framing due to the increased seismic demands the retrofit strategy may place on it. Specially designed light-gauge shear walls could provide engineers with an effective option to retrofit old buildings. Also, concentrically braced

frames are worth considering as a simple and effective retrofit system, especially when story drifts need to be limited. The concept is to design systems that are strong enough to resist the necessary seismic forces and yet light enough to keep the existing structural elements from needing further reinforcement. Additionally, if these systems could be installed quickly and eliminate the need to disrupt the occupants of existing structures, they would be even more desirable (in the context of a hospital retrofit for example).

Steel plate shear walls (SPSWs) are gaining acceptance as lateral load resisting systems, especially in seismic regions. By allowing the infill plates to buckle in shear, develop diagonal tension field action, and then dissipate energy through the cyclic yielding of the infills in tension, it has been shown that SPSWs can be useful seismic load resisting systems ([1–7], among many). However, the minimum

* Corresponding author at: Division of Theory of Structures, Faculty of Architecture, Istanbul Technical University, Taskisla, Taksim, Istanbul 34437, Turkey. Tel.: +90 212 293 1300x2293; fax: +90 212 251 4895.

E-mail addresses: jwberman@eng.buffalo.edu (J.W. Berman), celikoguz@itu.edu.tr (O.C. Celik), bruneau@mceermail.buffalo.edu (M. Bruneau).

hot-rolled plate thicknesses available for use in SPSWs often provide infill strengths greatly exceeding those required to meet code specified values [8], so the use of such infills for seismic retrofit would often require reinforcement of the existing beams and columns (or beam-to-column connections), which can be costly. Therefore, it would be advantageous to develop light-gauge SPSW systems.

Centrally braced frames (CBFs) are commonly used in new and retrofit construction to resist earthquakes by providing lateral stiffness, strength, and ductility. However, upon cyclic loading, progressive loss of compression strength and energy dissipation in compression results in less than ideal hysteretic loops. To improve the hysteretic characteristics of braces, cold formed steel studs (CFSSs) of the type often used in non-structural partition walls could be used to laterally restrain braces against buckling and enhance their seismic performance. This would require special design of CFSS members, to elastically resist the out-of-plane forces developing at the onset of brace buckling. Many theoretical and experimental studies have investigated the complex, inelastic cyclic behavior of steel braces, [9–12]. The slenderness ratio was deemed to have a most important impact on hysteretic behavior, and the use of stocky braces was recommended over slender braces.

While both of the above systems have merit in seismic retrofit applications, no guidance exists to help the engineer determine which of the two approaches is preferable in terms of providing stiffness, maximum displacement ductility, and cumulative hysteretic energy dissipation capacities for a given strength. In an attempt to provide some quantitative data for this purpose, this paper describes and compares the results from cyclic testing of six frames: four concentrically braced frames (two with CFSSs for in-plane and out-of-plane restraint of the braces and two without CFSSs), and two light-gauge SPSWs (one with a flat infill plate and one with a corrugated infill).

2. Experimental set-up

All test specimens used one of two boundary frames, which were modified as necessary to accommodate the different infills. All beam and column dimensions, as well as web-angle connections, were kept constant from specimen to specimen to allow a more uniform comparison of the strength, stiffness, and seismic energy dissipation capacity of the proposed retrofit strategies. Boundary frame dimensions were selected to be representative of bay dimensions for frames located in a test-bed structure called the “MCEER Demonstration Hospital” [13]. The boundary frame aspect ratio (L/h) of 2.0 is identical to that of the hospital’s structural system, where L and h are the bay width and height of the specimen respectively; however, the geometric scale of the boundary frame is 1/2 of the hospital’s framing due to limitations of the testing apparatus.

Two SPSW specimens (flat and corrugated infills) and four concentrically braced specimens were designed

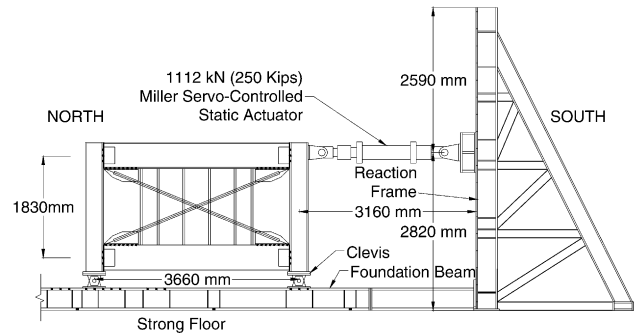


Fig. 1. Typical test set-up for specimens.

and constructed. Both square tubular and solid rectangular sections were used as brace members. Two of the specimens having concentric braces utilized closely spaced vertical CFSSs to reduce the buckling length of the braces, approaching to some degree (but not perfectly) the philosophy of buckling-restrained braced frames. All specimens were designed in the perspective of a seismic retrofit and to meet three major goals, namely, mobility, low impact on existing framing, and a substantial increase in energy dissipation capability compared to that of the existing framing. AISI [14], AISC LRFD Specifications [15], CAN/CSA-S16-01 [16], and AISC Seismic Provisions [17] codes were used during the design of these specimens. The specimen names and descriptions are:

- FP: Flat infill plate specimen with plate thickness of 1.0 mm (20 gauge).
- CP: Corrugated infill plate (cold formed steel deck) specimen with plate thickness of 0.75 mm (22 gauge).
- B1: CBF with single tube brace and vertical CFSSs spaced at 457.2 mm (18 in.) center-to-center.
- B2: CBF with single tube brace and without vertical CFSSs.
- B3: CBF with solid rectangular X-braces and vertical CFSSs spaced at 457.2 mm (18 in.) center-to-center.
- B4: CBF with solid rectangular X-braces and without vertical CFSSs.

A tall reaction frame located in the University at Buffalo’s Structural Engineering and Earthquake Simulation Laboratory (SEESL) was used to provide support for the lateral load applied to the specimens. This frame is rated to resist lateral loads of up to 1112 kN (250 kips) at a height of 2.4 m (8 ft) or lower. The test set-up for a typical specimen is shown in Fig. 1.

3. Materials

ASTM A572 Gr.50 steel was used for the boundary frame and its beam-to-column and column-to-base plate connections. The flat plate used in FP was ASTM A1008 (formerly A366) which is a cold rolled, carbon, commercial steel sheet. CP used steel deck produced by United Steel

Deck, Inc. as the infill material. This material conformed to ASTM A653 Grade 33 which is a galvanized material with a minimum yield stress of 230 MPa (33 ksi).

The tube material for B1 and B2 was ASTM A500 Gr.B with minimum yield stress of 317 MPa (46 ksi). The solid bar braces, gussets and angle connectors for the studs were ASTM A572 Gr.50. The U brackets, used as in-plane buckling restrainers, were ASTM A36 grade steel. Bolts used in the boundary frame connections (including those used for specimen mounting), SPSW infill connections to the boundary frames, and brace connections to the boundary frames were ASTM A490, while A307 grade bolts were used for other connections involved in the fabrication of Specimens B1, B2, B3, and B4. Locally available, 12 gauge, 228 MPa (33 ksi) yield point CFSS products were used in B1 and B3. Properties for the light gauge studs used here were taken from the Dietrich Product Data [18]. ASTM Standard coupon tests [19] for the SPSW infill plate materials were carried out and the resulting yield stresses were found to be 215 MPa for FP, and 325 MPa for CP. From similar coupon testing, the average values for the brace yield stresses were 377 and 385 MPa for the solid and tube braces, respectively.

The yield strength of the tube brace coupons was calculated using a 0.2% strain offset, because this steel exhibited no definite yield plateau. The solid bar coupons from the braces of B3 and B4 had an elastic–plastic behavior. Further details of coupon tests and their results can be found in [20] and [21]. Coupon tests were not performed for the boundary frame members as the beams and columns were designed to remain elastic. However, bare frame tests were carried out to characterize the cyclic behavior of the boundary frame alone since some inelastic action of the web-angle beam-to-column connections was expected.

This material data was employed in static pushover analyses of the specimens which, in turn, were used to approximate the load–displacement curves of the specimens prior to testing.

4. Details of specimens

The specimens constructed for this study are shown in Fig. 2(a) through (f). They were designed to be as large as possible without exceeding the maximum force capacity of 1112 kN (250 Kips) of the largest actuator available in the laboratory, with a safety factor of 1.50 and accounting for strain hardening effects. To maintain similarity to the gravity frames in the demonstration hospital, a double web-angle beam-to-column connection was designed following the procedures given in the AISC LRFD manual [22]. The bolts to the column flange were designed to be slip critical under the maximum actuator load with a safety factor of 2.0. Typical 8 mm fillet welds (all around the angle legs) to the beam web were used. Typical 5 mm fully circumferential fillet welds were used in the column-to-base plate connection. Six 38.1 mm ($1\frac{1}{2}$ ") diameter A490 bolts

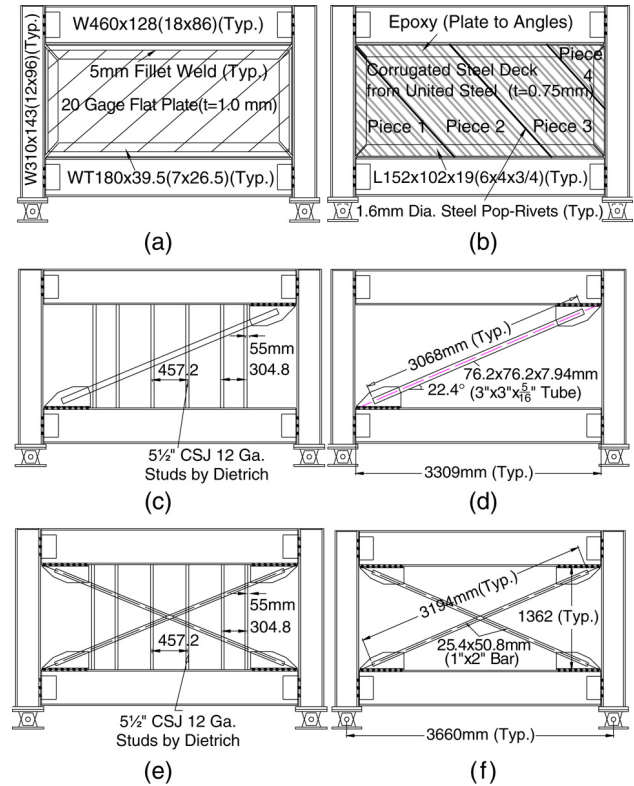


Fig. 2. Schematic of specimens: (a) FP; (b) CP; (c) B1; (d) B2; (e) B3; (f) B4.

were used to connect the 25.4 mm (1 in.) thick column base plates to the clevises and were designed to be slip-critical.

Several alternatives for the infill system-to-boundary frame connection details were experimentally sought during the design of the specimens. In the SPSW test specimens, since thin plates were selected, a bolted connection through the infill material was found impossible as it would have led to net section fracture governing over the gross section yielding of the plates (to dissipate energy, the plates must fully yield and non-ductile fracture modes must be avoided).

For the flat plate specimen, two different infill plate-to-boundary frame connections were employed. The first approach relied on an industrial strength epoxy. Although this connection performed satisfactorily during sub-assembly testing, it failed prior to infill yielding during actual specimen testing and will not be discussed further. The second approach (used for Specimen FP) relied on a continuous welded connection of the plate to the web of a WT180 × 39.5 (WT7 × 26.5). The flanges of the WTs were bolted to the flanges of the columns and beams using 29 mm diameter A490 bolts at 305 mm on center. These bolts were also designed to be slip-critical.

In CP, the plate was installed with the corrugations oriented at 45° with the horizontal. This was done to force the inclination angle of the tension field to be 45° (which corresponded to the calculated tension field angle for Specimen FP), and to delay the onset of buckling when the corrugations were in compression (as it was thought to be a

Table 1
Behavioral characteristics of tested specimens

Specimen	Total initial stiffness (kN/mm)	Initial stiffness-infill (kN/mm)	Yield or buckling base shear (kN)	Yield or buckling disp. (mm)	Max. drift (%)	μ	Total energy (kN m)	Infill energy (kN m)
FP	106.0	96.0	364.0	5.3	3.70	12	444	212
CP	93.0	86.0	518.0	8.1	1.40	3	73	50
B1	88.8	78.2	636.1	11.4	1.92	4	274	227
B2	61.4	51.0	511.5	10.2	2.88	6	310	192
B3	136.0	125.7	898.5	11.9	2.16	4	205	169
B4	106.6	96.3	182.4	3.0	2.16	4	95	37

possible advantage of this type of infill). Again several options for the connection were considered; finally, a connection in which the corrugated plate would be “sandwiched” between two angles, L152 × 102 × 19 (L6 × 4 × 3/4), that would be bolted to the boundary frame was considered. From sub-component testing of various mock-up connections, epoxy was determined to be the best way to connect the plate to the angles so that the yield strength of the infill plate could be developed. 29 mm diameter A490 bolts at 305 mm on center were chosen to connect the angles to the boundary frame. Due to the maximum available steel deck width of 910 mm, it was necessary to fabricate the infill plate for this specimen in four separate pieces as shown in Fig. 2(b). These pieces were fastened together using 1.6 mm diameter steel pop-rivets at a spacing of 101.6 mm on center. Additional details for SPSW specimens can be found in [7,20].

In the braced frame specimens, a single tube brace of 76.2 mm by 76.2 mm (3 in. × 3 in.) with $t = 7.94$ mm (5/16 in.) wall thickness, and solid X braces having a cross section of 25.4 mm by 50.8 mm (1 in. × 2 in.), were selected. The tube braces had 431.8 mm long and 12.7 mm wide slots at each end for welded connection to gussets.

All CFSSs used in B1 and B3 were 5½” CSJ 12 gauge by Dietrich [18]. Their sectional dimensions were determined to resist the forces generated by the braces at the onset of buckling in the out-of-plane direction. Details for CFSS-to-beam connections and U brackets used as in-plane buckling restrainers can be found in [21].

All specimens were instrumented with strain gauges, tomposonics, and potentiometers.

5. Testing

Quasi-static cyclic testing was performed in accordance with the ATC-24 [23] testing protocol. During all tests, the top horizontal displacement of the specimens was taken as the displacement control parameter. The yield displacement for each specimen was theoretically estimated from numerical simulation using pushover analysis (with actual material properties from the coupon tests and assuming simple beam-to-column connections). Elastic cycles (i.e. 1/3 and 2/3 of yield) were essentially based

on these estimates; however, for the inelastic cycles, since there was slight variation between the theoretical and experimental yield values, the experimentally obtained yield displacement was used as a basis.

In Specimens B1 through B4, special care was taken during the tests to identify the point of buckling initiation for the braces. To facilitate comparison between the results obtained for B1 and B2, the same cyclic displacement history that was applied to B1 (i.e. absolute displacement values) was applied to B2. Again, to facilitate comparisons between B3 and B4, the same cyclic displacement history that was applied to B3 was applied to B4.

6. Experimental observations

The behavior of each specimen, both in the elastic and inelastic ranges, is described below. Using experimental hystereses, total initial stiffness, initial stiffness of infill, yield or buckling base shear, yield or buckling displacement, maximum attained percent drift, achieved displacement ductility, and cumulative energy dissipations (total and infill-only) are quantified in Table 1.

6.1. Specimen FP

Specimen FP exhibited linear behavior during the first six cycles of testing. At 0.29% drift (the first half of Cycle 7), audible buckling sounds began and the magnitude of the buckling waves became visible. This specimen was successfully tested to 82.6 mm of displacement ($12\delta_y$, 3.7% drift). The maximum base shear was 660 kN which occurred at $10\delta_y$. Fractures developed at the corners of the infill plate and propagated along the fillet welds that connected the infill plate to the intermediate WTs. Although the infill plate could still carry some load in spite of its extensive damage, testing stopped when the angles of the beam-to-column connections of the boundary frame suffered large fractures at frame displacements of $12\delta_y$. Fig. 3(a) shows the buckling of the infill and formation of the diagonal tension field at the maximum displacement ductility reached.

The hysteresis for Specimen FP is shown in Fig. 4(a) superimposed with the hysteresis of the bare frame modeled as described in [20,21]. The overall behavior of FP was

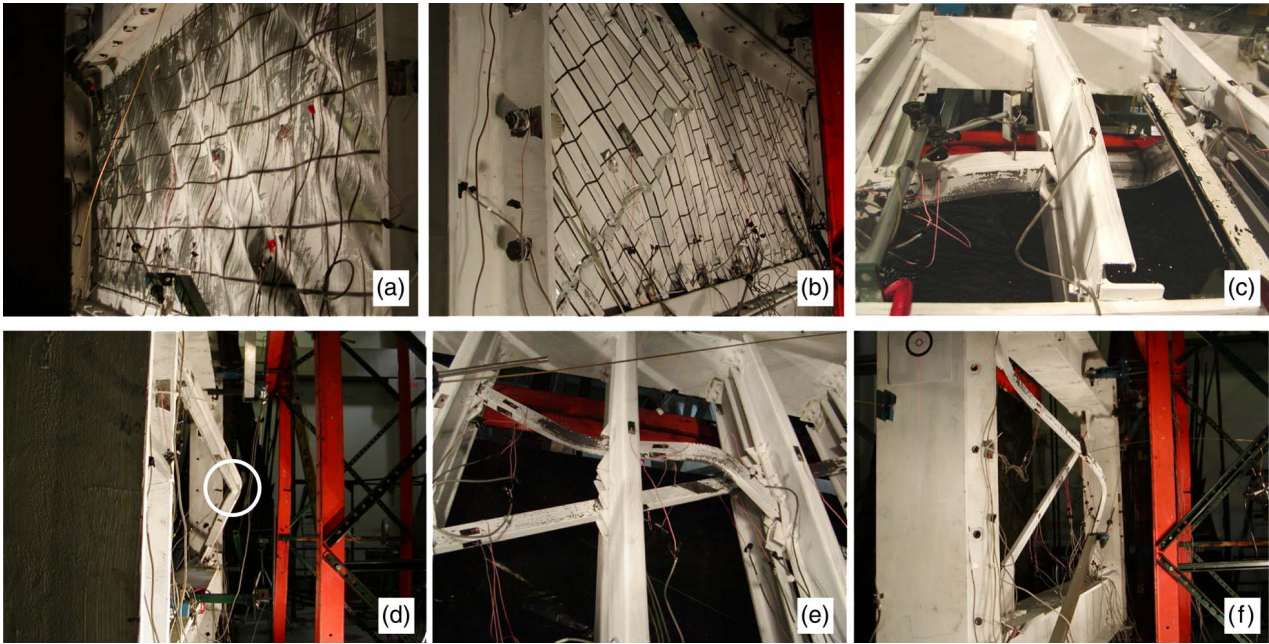


Fig. 3. Damage level in specimens: (a) FP (12 δ_y , Cycle 29); (b) CP (3 δ_y , Cycle 16); (c) B1 (-4 δ_y , Cycle 16); (d) B2 (-5 δ_y , Cycle 21); (e) B3 (-4 δ_y , Cycle 19); (f) B4 (-4 δ_y , Cycle 19).

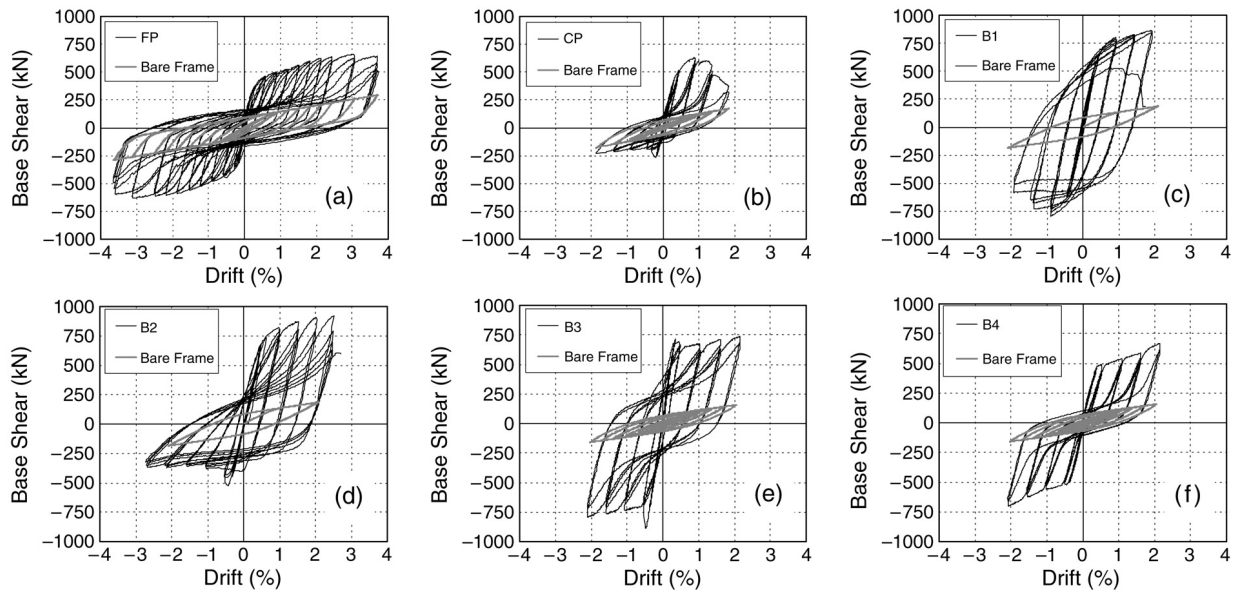


Fig. 4. Experimental hysteresis curves for specimens and bare frames: (a) FP; (b) CP; (c) B1; (d) B2; (e) B3; (f) B4.

ductile and stable up to large drift levels, although significant pinching is apparent in the hysteretic loops. Fig. 5(a) shows the hysteresis of the infill alone (i.e. after subtracting the bare frame's contribution). Table 1 shows that 90% of the initial stiffness of the system is due to the contribution of the infill. Also of interest in Table 1 is the substantial amount of energy dissipated by the infill. The strain gauge data obtained showed that the strain was fairly uniform across the infill, indicating that the entire plate participated in dissipating energy.

6.2. Specimen CP

The hysteretic behavior of Specimen CP was elastic during the first three cycles of testing. Some popping noises were heard during the elastic cycles. Local buckling began to occur during Cycle 7 and progressed in the subsequent cycles. Residual buckles were visible at zero displacement during the three cycles at the yield displacement of 8.1 mm (0.44% drift, Cycle 10). Epoxy cracking along the connection to the bottom beam was observed at

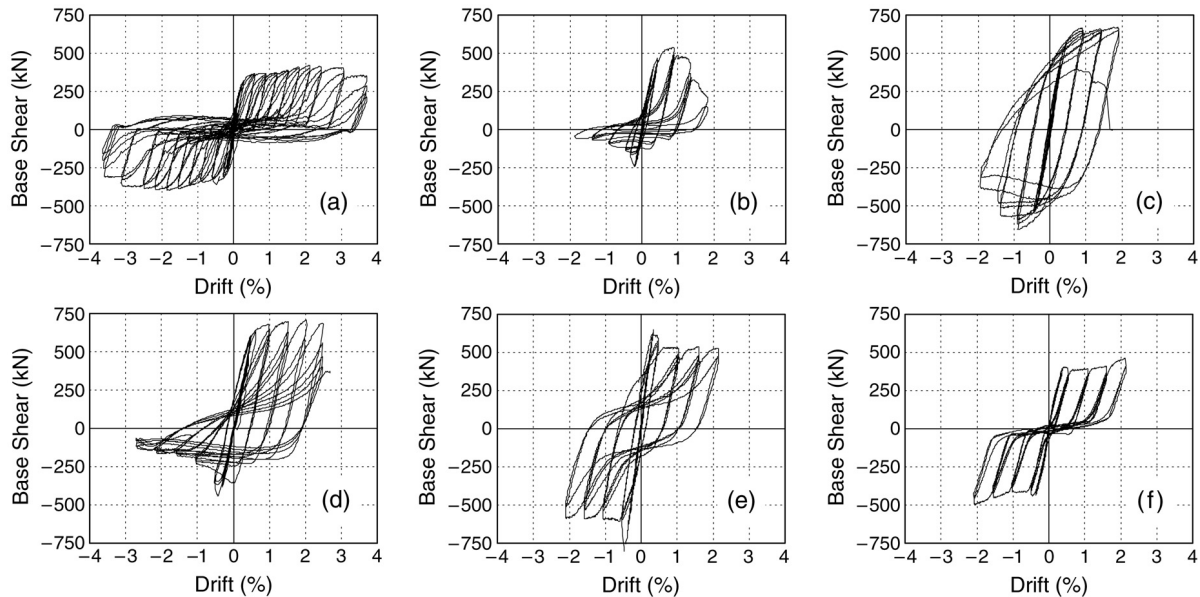


Fig. 5. Base shear versus drift hysteresis curves for infills (a) FP; (b) CP; (c) B1 ($KL/r = 19.7$); (d) B2 ($KL/r = 77.3$); (e) B3 ($KL/r = 65.5$); (f) B4 ($KL/r = 195.7$).

the end of the three cycles at the yield displacement. Additionally, some pop-rivets failed at the end of the $\pm 1\delta_y$ cycles. However, there was no significant change in the maximum base shear obtained during these cycles. Subsequent displacement cycles increased the amount of local buckling along two distinct lines that were visible on the infill plate, initiating fractures along them. Epoxy cracks propagated further, and the loss of additional pop-rivets resulted in visible separations between the two infill plate pieces. Specimen CP was successfully tested to a maximum displacement of 40.6 mm ($4\delta_y$, 2.2% drift). Failure of the specimen was from fractures of the infill plate at locations of repeated local buckling. Shown in Fig. 3(b) is the local and global infill buckling at $-3\delta_y$.

Fig. 4(b) shows the hysteresis for CP and the bare frame. As expected, the hysteresis for CP is one-sided because tension field action only occurred when the corrugations were in tension. The rapid degradation in strength observed following the cycles at $3\delta_y$ (1.4% drift) was due to the severe local buckling and fractures that developed during negative loading. Fig. 5(b) shows the hysteresis after the subtraction of the boundary frame contribution. Although pinching in the curves is evident, the infill contributed to the energy dissipation capability of the system. Table 1 shows that more than 67% of the total energy dissipated during the test was dissipated by the infill versus 33% for the boundary frame. Also shown in Table 1, the contribution of the infill to the initial stiffness was over 90%. Furthermore, a displacement ductility (μ) of 3 was achieved as the strength of the system was 91% of the maximum strength achieved, of which approximately 74% was taken by the infill and 26% by the boundary frame. At $\mu = 2$, the specimen achieved its maximum strength of 633 kN.

6.3. Specimen B1

Up to 0.96% drift ($2\delta_y$), B1 did not show significant deterioration in strength and stiffness; the behavior was almost cyclic symmetric with comparable axial yielding in tension and compression. B1 exhibited ductile, stable, and unpinched hysteretic behavior mainly provided by the existence of the CFSS members. These members and U brackets prevented out-of-plane and in-plane brace buckling at the early stages of cyclic loading. After several cycles at displacement levels greater than the yield displacement, bearing failure of the intermediate studs led to loss of contact between the buckling restrainers and the brace, which resulted in reduced base shear strength and system stiffness. A general view from the specimen at $-4\delta_y$ is shown in Fig. 3(c). This test was terminated when the brace fractured.

Experimental base shear force versus drift hysteresis curves for B1 and the bare frame are shown in Fig. 4(c). Results for the case of infill-only are illustrated in Fig. 5(c). The shape of the hysteresis for B1 gradually becomes one-sided upon repeated inelastic buckling of the tubular brace member. However, the difference between the buckling and tension strengths in each cycle is still significantly less than would be expected in absence of lateral bracing by the studs.

Strain gauge data obtained showed that 2% strain was reached in the brace at 1.92% drift. A displacement ductility ratio (μ) of 4 was achieved when the tension and compression strengths of the specimen were, respectively, 100% and 67% of the maximum values obtained experimentally. As seen from Table 1, the contribution of the infill to the initial stiffness was 88%, and 83% of the total energy dissipated by the infill versus 17% for the boundary frame.

6.4. Specimen B2

Up to 0.48% drift, the hysteresis curves for B2 are cyclic symmetric; however, in the aftermath of brace buckling, they become one-sided due to the deterioration in buckling strength. On the tension side, strength increases until fracture develops. Fig. 3(d) shows the buckled brace at $3\delta_y$. The base shear force versus drift hysteresis for B2 is shown in Fig. 4(d) superimposed with the hysteresis of the bare frame. Results for the case of infill-only are illustrated in Fig. 5(d). B2 exhibited ductile and stable cyclic behavior up to 2.40% drift, although some pinching is obvious in the hystereses. This test was terminated when the brace fractured.

Table 1 shows that the contribution of the brace to the initial stiffness was 83%. Appreciable energy was dissipated after the elastic cycles, and increased in the following cycles. As indicated in Table 1, 62% of the total hysteretic energy was dissipated by the infill versus 38% for the boundary frame.

6.5. Specimen B3

Up to approximately 0.50% drift, the specimen did not show deterioration in strength and stiffness. At the onset of buckling of the east side brace segment between the fourth and the fifth studs (counting from the north), the base shear dropped abruptly. The peak base shear force during the test was reached prior to this buckling. Fig. 3(e) shows the classical buckled shape of the braces at $4\delta_y$. Experimental base shear force versus drift hysteresis curves for B3 and the bare frame are shown in Fig. 4(e). The loops after subtracting the contribution of the bare frame are illustrated in Fig. 5(e). After buckling, the hysteresis for B3 stabilizes and fuller curves, relative to B4, develop in both the positive and negative drift regions. For negative and positive base shears, absolute ratios of the maximum negative and positive base shears at final cycles to the peak base shear at brace buckling are 0.89 and 0.83 respectively.

The overall behavior of B3 was ductile and stable up to 2.16% drift, although pinching in the hysteretic loops is apparent. Out-of-plane displacement demand was significantly constrained by the presence of CFSSs. This test was terminated to prevent damage to the beam-to-column connections of the boundary frame which had to be used again in subsequent testing.

6.6. Specimen B4

B4 exhibited a displacement ductility ratio (μ) of 4. No significant energy was dissipated during the elastic cycles, and starting from the brace yielding cycle, the cumulative energy dissipated increased. Shown in Fig. 3(f) is the out-of-plane buckling view of the compression brace, from when the tension brace elongation was $4\delta_y$. Fig. 4(f) shows experimental base shear force versus drift hysteresis curves

for B4 and the bare frame. The hysteresis for Specimen B4 is fairly symmetrical in the elastic and inelastic cycles and the behavior after subtracting the contribution of the bare frame is illustrated in Fig. 5(f). The overall behavior of Specimen B4 was ductile and stable up to 2.16% drift, although significant pinching is visible in the hystereses. The test was also terminated to prevent damage to the beam-to-column connections of the boundary frame.

A strain of 1.7% was reached in the bar braces at 2.16% drift. Hysteretic loops show that energy was dissipated by tension yielding rather than brace buckling. Table 1 reveals that only 39% of the total energy was dissipated by the infill versus 61% for the boundary frame. The contribution of the boundary frame to cumulative energy dissipation is dominant over the infill at larger drifts, due to the inelastic behavior of the beam-to-column double angle connections. Strain gauges mounted on the boundary frame beams and columns showed those members remained elastic for all tests, as per the design intent.

7. Summary

All specimens underwent inelastic reversed cyclic displacement histories prior to initiation of fracture. The maximum drift was reached by FP, at 3.70%. Specimens CP, B1, B2, B3, and B4 exhibited maximum drifts of 1.40%, 1.92%, 2.88%, 2.16%, and 2.16% respectively (although not all tests were stopped for the same reasons, as described above). Additional experimental data and details (including the strain gauge recordings and out-of-plane displacements of the braces) can be found in [20,21].

Specimen CP performed well and dissipated a relatively moderate amount of hysteretic energy while providing stable, albeit pinched, hysteretic behavior up to a displacement ductility of 3. The entire infill was active in dissipating energy. An epoxy connection proved adequate to connect the corrugated infill to the boundary frame, allowing the specimen to reach its ultimate failure by fracture of the infill at locations of repeated local buckling. Superior behavior for SPSWs was achieved by Specimen FP, as evidenced by the significant hysteretic energy dissipated and the large displacement ductility reached. Again, the entire plate contributed to the energy dissipation. Specimen FP is also the simplest SPSW system to construct of the two configurations investigated here.

Specimen B1 achieved superior behavior over the other braced frame specimens in terms of infill cumulative hysteretic energy dissipation at given drift values. The cumulative energy dissipation of the infill for this specimen was 18% more than that of Specimen B2 (without studs). However, maximum displacement ductilities (μ) of Specimens B1 and B2 are 4 and 6, respectively. The experimental fracture life of the tube in Specimen B2 was higher than that of the tube in Specimen B1, as reducing the buckling length for tubular cross section braces also accelerated their local buckling. If hysteretic energy is

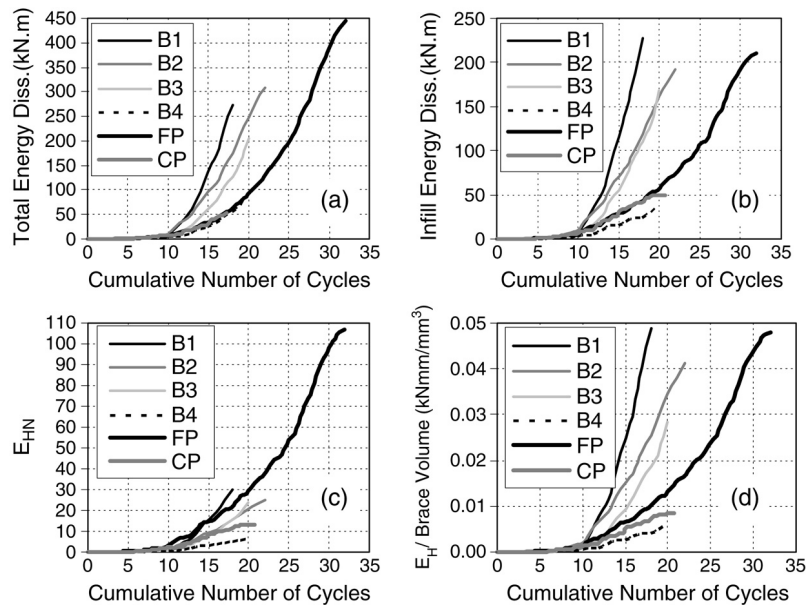


Fig. 6. Comparison of cumulative energy dissipation for specimens: (a) total frame; (b) infill-only; (c) normalized cumulative energy dissipation (infill-only); (d) cumulative energy dissipation per infill volume used.

instead calculated and compared at a given ductility level, for example at the ductility level at which the tube brace fractured in Specimen B1, then 92% more hysteretic energy is dissipated in Specimen B1, compared to Specimen B2. Initial stiffness and base shear at yield for Specimen B2 are about 65% and 80% of those of Specimen B1, respectively.

At the maximum displacement ductility of 4, infill cumulative energy dissipation for Specimen B3 reached 4.57 times the energy dissipated in Specimen B4, a 357% gain in infill energy dissipation. From this perspective, the use of CFSSs and U brackets as buckling restrainers seemed more effective in tension-only braced frames rather than tension-compression braced frames. Moreover, provided that all brace connections are ductile, solid braces may be able to sustain larger amounts of reversed axial cyclic displacements, since local stability problems do not exist. While the ratio of maximum total base shears reached by Specimens B3 and B4 is 1.28, this value is 4.93 at initial brace buckling. In other words, the maximum base shear strength is developed in Specimen B3 at initial brace buckling, but maximum strength of Specimen B4 is developed at maximum ductility instead.

8. Cumulative energy dissipation and comparison

A comparison of the hysteretic behavior of all specimens is made easier by Fig. 5(a) through (f). Using experimental hystereses, the variation of cumulative energy dissipation (total and infill-only) with cumulative number of cycles for all specimens is shown in Fig. 6(a) and (b).

Following the procedure given below, to better compare the effectiveness of each specimen, normalized values

of base shear and energy dissipation (infill-only) were calculated and summarized in Table 2.

Cumulative hysteretic energy dissipation can be normalized as follows:

$$E_{HN} = \frac{E_H}{V_y \delta_y} \quad (1)$$

where E_{HN} = normalized cumulative hysteretic energy dissipation, E_H = cumulative hysteretic energy dissipation, V_y = yield (or buckling) base shear, and δ_y = experimentally obtained yield (or buckling) displacement. Note that, for the purpose of normalization, the average of the base shear reached in tension at each of the large plastic deformation cycles was used for the value of V_y . The variation of normalized cumulative energy dissipation with cumulative number of cycles for all specimens is shown in Fig. 6(c). Table 3 gives the cycle number and corresponding ductility level for each specimen for reference since the cumulative energy dissipation is plotted against cumulative cycle number.

Table 2 shows that the flat plate shear wall and the braces having CFSS members had larger normalized hysteretic energy dissipation. Total and normalized cumulative hysteretic energies were the greatest in Specimen FP, although significant pinching in the hysteresis is apparent. Specimen B1 achieved the maximum hysteretic energy dissipation for the infill alone, although this specimen had less maximum displacement ductility due to its lower fracture life as compared to Specimen B2. Energy dissipation amounts by the infills of other specimens were 93%, 22%, 85%, 74%, and 16% of Specimen B1's energy dissipation for Specimens FP, CP, B2, B3, and

Table 2
Normalized characteristics of tested specimens (infill-only)

Specimen	V_y (kN)	δ_y (mm)	$E_{H,infill}$ (kN mm)	$V_y/(V_{y,B2})$	$E_{H,infill}/E_{H,infill,B1}$	E_{HN}
FP	371.0	5.3	211,000	0.55	0.93	107.3
CP	460.0	8.1	50,000	0.68	0.22	13.4
B1	661.3	11.4	227,000	0.98	1.00	30.1
B2	673.0	11.4	192,000	1.00	0.85	25.0
B3	592.3	11.9	169,000	0.88	0.74	24.0
B4	442.0	11.9	37,000	0.66	0.16	7.0

Table 3
Ductility levels reached at different cycles for tested specimens

Cycle number	Specimen Δ/δ_y					
	B1 ^a	B2 ^a	B3	B4	FP	CP ^a
1–3	0.33	0.33	0.2	0.2	0.25	0.17
4–6	0.67	0.67	0.43	0.43	0.64	0.42
7–9	1	1	0.76	0.76	1	0.7
10–12	2	2	1	1	2	1
13–15	3	3	2	2	3	2
16–17	4	4	3	3	4	3
18	–	5	3	3	5	3
19	–	5	4	4	5	4
20	–	5	4	4	6	4
21	–	5	–	–	6	–
22	–	6	–	–	7	–
23	–	–	–	–	7	–
24	–	–	–	–	8	–
25	–	–	–	–	8	–
26	–	–	–	–	10	–
27	–	–	–	–	10	–
28	–	–	–	–	12	–
29	–	–	–	–	12	–
30	–	–	–	–	12	–
31	–	–	–	–	12	–

^a The final cycles for these specimens were 1/2 cycles due to fracture and strength degradation.

B4 respectively. Similarly, percentage average base shear strengths of the specimens are also given in Table 2.

Of the braced frames, Specimen B2 dissipated the largest amount of total hysteretic energy, essentially due to its longer fracture life. The out-of-plane buckling displacements of the brace were significant, in excess of 10% of the brace clear length. Although residual out-of-plane displacements caused significant strength degradation in compression, the behavior was ductile and stable.

Specimen B3 performed well and dissipated significant energy with ductile but pinched hysteretic curves. Up to displacement ductility of 4, the braces dissipated energy by yielding and buckling under reversed displacement cycles. CFSS members and U brackets reduced the buckling length of the braces effectively.

Specimen B4 dissipated the least amount of infill and normalized cumulative energies. The hysteresis curves were stable yet significantly pinched, as expected. Energy was essentially dissipated through the yielding of the braces in tension only. A displacement ductility of 4 was reached

without any visible damage. Note that the largest out-of-plane displacements were obtained for this specimen, in excess of 14% of the brace clear length.

Hysteretic energy dissipation per infill material volume used can be another measure to compare the relative effectiveness of the tested specimens. Shown in Fig. 6(d) is the variation of volumetric energy dissipation versus cumulative number of cycles. Peak energy per volume values of 0.048, 0.008, 0.049, 0.041, 0.028, and 0.006 kN mm/mm³ are found for Specimens FP, CP, B1, B2, B3, and B4 respectively (although the last two specimens were not tested to failure), which shows that FP, B1 (with studs), and B3 (with studs) dissipated the most energy per unit volume of material.

It is also useful to compare the energy dissipated by the various infills at the same ductility level, $\mu = 3$ for example, which is close to what is implied in the R values for SPSWs in simple frames and concentrically braced steel frames. Table 4 shows the experimental results for total, infill-only, normalized, and volumetric energies dissipated by the specimens considered in this study. From that table, it is understood that Specimens B1 (with CFSSs), B3 (with CFSSs), and FP are more effective than the others in terms of the energy dissipated by their infills at a common ductility of $\mu = 3$ since their normalized cumulative energy dissipations are the largest. As for the volumetric energy dissipation at $\mu = 3$, again Specimen B1 is superior over the other five specimens.

Another interesting comparison regarding specimen energy dissipation can be made if the specimen hystereses are scaled to the same design base shear for the infill-only (i.e. after subtraction of the boundary frame contribution). For Specimens B3 and B4, the design base shear can be taken as the base shear of the system (considering both braces) when brace yielding occurs, which corresponds to 640 and 400 kN, respectively. This has the advantage of corresponding to the plateau on the backbone curve of the hysteresis following the initial peak due to higher compression strength at first buckling. The design base shear is similarly defined for Specimen FP, which is 340 kN. However, for Specimens B1 and B2, which each had a single tubular brace, the base shear at brace buckling and the base shear at brace yield are added to give the design base shear, resulting in design base shears of 1075 and 1020 kN respectively. This is done because

Table 4
Hysteretic energy dissipated at the ductility level of $\mu = 3$

Specimen	Cum. no. of cycles	Drift at $\Delta/\Delta_y = 3$ (%)	$E_{H,Total}$ (kN m)	$E_{H,Total}/E_{H,Total,B1}$	$E_{H,Infill}$ (kN m)	$E_{H,infill}/E_{H,infill,B1}$	E_{HN}	$E_{HN}/E_{HN,B3}$	$E_H/vol.$ (kN mm/mm ³)	$(E_H/vol.)/(E_H/vol.)_{,B1}$
FP	15	0.90	34.6	0.26	29.0	0.25	14.7	0.94	0.0066	0.27
CP	18	1.38	58.2	0.43	43.3	0.37	11.7	0.75	0.0072	0.29
B1	15	1.44	135.0	1.00	116.0	1.00	15.4	0.98	0.0249	1.00
B2	15	1.44	95.2	0.71	70.7	0.61	9.2	0.59	0.0152	0.61
B3	18	1.62	128.0	0.95	111.0	0.96	15.7	1.00	0.0187	0.75
B4	18	1.62	54.8	0.41	24.7	0.21	4.7	0.30	0.0042	0.17

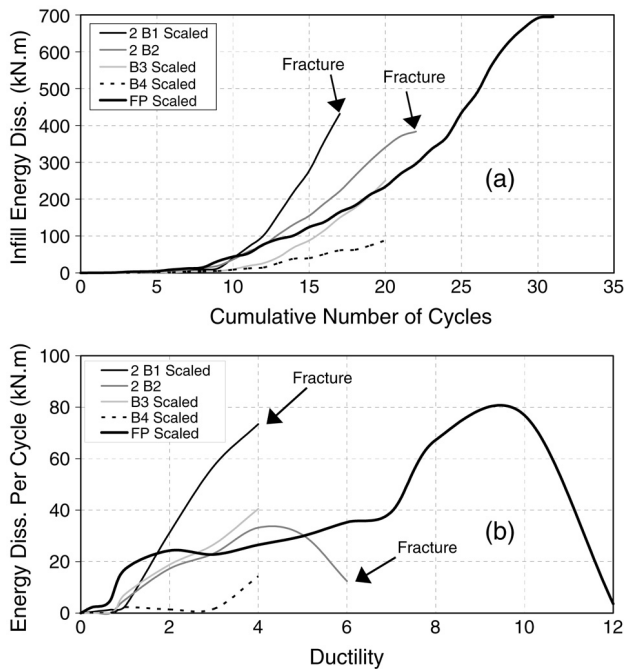


Fig. 7. (a) Cumulative energy dissipation of specimens after scaling to the same design base shear; (b) energy dissipation per cycle versus ductility of scaled specimens (using the last cycle at each displacement level).

seismic design requirements would mandate that a brace acting in compression be complemented by at least one brace simultaneously acting in tension along a specific frame line. Arbitrarily selecting the design base shear of Specimen B2 as a reference results in scale factors of 0.95, 1.594, 2.55, and 3, for Specimens B1, B3, B4, and FP, respectively. The hysteresis of each specimen was multiplied by the corresponding scale factor and the cumulative energy dissipation of the resulting scaled hysteresses was calculated. The results are shown against the cumulative number of cycles in Fig. 7(a). Note that the cumulative energy dissipation for Specimens B1 and B2 calculated after the hysteresses were scaled, for a single tubular brace, has been doubled to be consistent with the explanation given above and that these will be referred to as 2B1 and 2B2.

As shown in Fig. 7(a), similar cumulative energy dissipation is achieved for the steel plate shear wall Specimen FP, and the braced frames with two tubular

braces (2B2) or braced frames with two solid braces and CFSSs (B3). However, fracture from local buckling occurred in the tubular braces. Specimen 2B1, which had more cumulative energy dissipation than Specimens FP, 2B2, and B3, also suffered fracture at a lower ductility level since local buckling was accelerated by the lateral restraint of the CFSSs.

Fig. 7(b) shows the variation in energy dissipation per cycle, using information from the final cycle at each displacement level, versus the maximum ductility reached during that same cycle. Again, Specimens FP, 2B2, and B3 exhibit similar energy dissipation per cycle up to a ductility of 4. Beyond that point, the energy dissipated per cycle by Specimen FP continues to increase while for Specimen 2B2 it decreases until the brace fractured. Note that for Specimen B3 the testing was stopped after the cycles at a ductility of 4 and the behavior beyond that ductility is not known. Additionally, Specimen 2B1 dissipated an increasing amount of energy until the last cycle (at a ductility of 4), when it fractured.

From Fig. 7(a) and (b), it appears that flat plate steel shear walls (FP) have similar energy dissipation capacity, both in terms of cumulative energy dissipation and energy dissipation per cycle, as braced frames with two tubular braces (2B2), or braced frames with two solid braces and CFSSs (B3), while providing a longer fracture life than tubular braces.

Experiments conducted in this study also showed that Specimen B3 provides greater initial stiffness and strength, and that Specimen FP had the maximum displacement ductility. Additionally, local buckling and fracture are less of a concern in steel plate shear walls with flat infills.

Note that observations on ultimate system performance depend on the fracture life of the components subjected to large plastic deformations, for which some statistical variations are expected. This variability may affect some quantities reported here, such as maximum drift. This is why the behaviors of the specimens were compared not only at maximum drift levels but at a ductility of 3 as well, which is achievable for all systems considered.

Finally, note that all specimens considered in this research used inexpensive infills. Therefore, labor costs likely dominate the total fabrication costs. Since labor costs

vary significantly regionally, the design engineer should work closely with the contractors to determine which of these solutions that meet the performance goals would be the most cost-effective to implement.

9. Conclusions

In this study, the behavior of specially designed braced frames and steel plate shear walls has been compared using experimental results. Six specimens, four braced frames and two SPSWs were designed, constructed, and experimentally tested using similar loading regimes. Two of the braced frames had single tubular braces, one with CFSSs for in-plane and out-of-plane restraint of the braces (B1) and one without CFSSs (B2), while the other two braced frames had solid bar braces in an X configuration, one with CFSSs (B3) and one without CFSSs (B4). One SPSW specimen used a flat infill plate (FP) and one used a corrugated infill plate (CP).

Using the experimental hystereses, it was found that Specimen B3 had the largest initial stiffness, and Specimen FP achieved the largest ductility. Upon scaling the hysteretic results to the same design base shear, it was found that both the energy dissipated per cycle and the cumulative energy dissipation were similar for steel plate shear walls with flat infills and braced frames with two tubular braces, up to a ductility of 4. After that, the tubular braces fractured while the SPSW with a flat infill reached a ductility of 9 before the energy dissipation per cycle decreased.

Acknowledgements

This research was supported in part by the Earthquake Engineering Research Centers Program of the National Science Foundation (NSF) under Award Number EEC-9701471 to the Multidisciplinary Center for Earthquake Engineering Research (MCEER). The second author thanks the Istanbul Technical University (ITU) President Office and ITU Faculty of Architecture for their partial support during his stay in Buffalo, under Grant to Support Long Term Research Activities Abroad for Young Researchers. However, any opinions, findings, conclusions, and recommendations presented in this paper are those of the authors and do not necessarily reflect the views of the sponsors.

References

- [1] Thorburn LJ, Kulak GL, Montgomery CJ. Analysis of steel plate shear walls. Structural engineering report no. 107, Department of Civil Engineering, University of Alberta, Edmonton, Alberta, Canada; 1983.
- [2] Timler PA, Kulak GL. Experimental study of steel plate shear walls. Structural engineering report no. 114, Department of Civil Engineering, University of Alberta, Edmonton, Alberta, Canada; 1983.
- [3] Caccese V, Elgaaly M, Chen R. Experimental study of thin steel-plate shear walls under cyclic load. *J Struct Eng ASCE* 1993;119(2): 573–87.
- [4] Driver RG, Kulak GL, Kennedy DJL, Elwi AE. Seismic behavior of steel plate shear walls. Structural engineering report no. 215, Department of Civil Engineering, University of Alberta, Edmonton, Alberta, Canada; 1997.
- [5] Elgaaly M. Thin steel plate shear walls behavior and analysis. *Thin Walled Struct* 1998;32:151–80.
- [6] Lubell AS, Prion HGL, Ventura CE, Rezai M. Unstiffened steel plate shear wall performance under cyclic loading. *J Struct Eng ASCE* 2000;126(4):453–60.
- [7] Berman JW, Bruneau M. Experimental investigation of light-gauge steel plate shear walls. *J Struct Eng ASCE* 2004 [in press, scheduled for vol. 131, No. 2].
- [8] Timler P. Design procedures development, analytical verification, and cost evaluation of steel plate shear wall structures. Technical report no. 98-01, Earthquake Engineering Research Facility, University of British Columbia, Vancouver, British Columbia, Canada; 1998.
- [9] Black RG, Wenger WAB, Popov EP. Inelastic buckling of steel struts under cyclic load reversals. Report no. UCB/EERC-80/40, Berkeley, CA; 1980.
- [10] Ikeda K, Mahin SA. A refined physical theory model for predicting the seismic behavior of braced steel frames. Report no. UCB/EERC-84/12, Berkeley, CA; 1984.
- [11] Tremblay R. Inelastic seismic response of steel bracing members. *J Construct Steel Res* 2002;58:665–701.
- [12] Tremblay R, Archambault MH, Filiatrault A. Seismic response of concentrically braced steel frames made with rectangular hollow bracing members. *J Struct Eng ASCE* 2003;129(12):1626–36.
- [13] Yang TY, Whittaker A. MCEER demonstration hospitals-mathematical models and preliminary results. Technical report, Multidisciplinary Center for Earthquake Engineering Research, University at Buffalo, Buffalo, NY; 2002.
- [14] American iron and steel institute (AISI). Cold-formed steel design manual. Washington, DC; 1996.
- [15] American institute of steel construction (AISC). Load and resistance factor design (LRFD) specification for structural steel buildings. Chicago, IL; 1999.
- [16] Canadian standards association (CSA). Limit states design of steel structures. CAN/CSA S16-01. Willowdale, Ontario, Canada; 2001.
- [17] American institute of steel construction (AISC). Seismic provisions for structural steel buildings. Chicago, IL; 2003.
- [18] Dietrich industries, Inc. Curtain wall/light gage structural framing products. ICBO No. 4784P. LA RR No. 25132; 2001.
- [19] American society for testing and materials (ASTM). Standard test methods and definitions for mechanical testing of steel products. A 370-97a. Philadelphia, PA; 2002.
- [20] Berman JW, Bruneau M. Experimental investigation of light-gauge steel plate shear walls for the seismic retrofit of buildings. Technical report MCEER-03-0001, Multidisciplinary Center for Earthquake Engineering Research, Buffalo, NY; 2003.
- [21] Celik OC, Berman JW, Bruneau M. Cyclic testing of braces laterally restrained by steel studs to enhance performance during earthquakes. Technical report MCEER-04-0003. Multidisciplinary Center for Earthquake Engineering Research, Buffalo, NY; 2004.
- [22] American institute of steel construction (AISC). Manual of steel construction. Load and resistance factor design. 3rd ed. Chicago, IL; 2001.
- [23] Applied technology council. ATC-24/Guidelines for cyclic seismic testing of components of steel structures. California; 1992.